ICES REPORT 10-23

June 2010

Solution of Dual-Mixed Elasticity Equations using Arnold-Falk-Winther Element and Discontinuous Petrov-Galerkin Method, a Comparison

by

J. Bramwell, L. Demkowicz and W. Qiu

The Institute for Computational Engineering and Sciences
The University of Texas at Austin
Austin, Texas 78712

Reference: J. Bramwell, L. Demkowicz and W. Qiu, "Solution of Dual-Mixed Elasticity Equations using Arnold-Falk-Winther Element and Discontinuous Petrov-Galerkin Method, a Comparison", ICES REPORT 10-23, The Institute for Computational Engineering and Sciences, The University of Texas at Austin, June 2010.

SOLUTION OF DUAL-MIXED ELASTICITY EQUATIONS USING ARNOLD-FALK-WINTHER ELEMENT AND DISCONTINUOUS PETROV-GALERKIN METHOD, A COMPARISON

J. Bramwell, L. Demkowicz and W. Qiu

Institute for Computational Engineering and Sciences
The University of Texas at Austin, Austin, TX 78712, USA

Abstract

Key words: convection-dominated diffusion, hp-adaptivity, Discontinuous Petrov Galerkin

AMS subject classification: 65N30, 35L15

Acknowledgment

Demkowicz and Bramwell were supported in part by the Air Force Office of Scientific Research contract FA9550-09-1-0608 (P.I. Omar Ghattas).

1 Introduction

Construction of stable Finite Element (FE) discretizations for the dual-mixed system of linear elasticity has been an area of research for three decades [11, 1, 2, 26, 27, 3, 28, 20, 25, 19, 4, 5, 18, 10]. The recent element of Arnold, Falk and Winther [4, 5, 18] builds upon reproducing on the discrete level an exact sequence for the elasticity equations with weakly imposed symmetry. The sequence lays a foundation for stability of the continuous problem. Constructing its discrete counterpart is more complicated than for the classical grad-curl-div sequence where the $H^1, H(\text{curl}), H(\text{div})$ spaces are replaced with polynomial spaces corresponding to Lagrange, Nédélec and Raviart-Thomas elements, but the grad-curl-div operators remain unchanged. Besides the differential operators, the elasticity complex involves purely algebraic operations which have to be replaced for the discrete spaces with judiciously designed approximations. In the end, the proof of discrete stability reduces to the construction of appropriate interpolation operators that make simultaneously commute three particular diagrams related to the elasticity complex.

The AFW element has been recently extended to elements of variable order [22, 23, 24]. Whereas the generalization of polynomial spaces is standard, see [12, 17], the construction of the interpolation operators

is not, and it is rather technical. 2D numerical experiments confirm the stability not only for h-refined meshes of variable order, but for hp-refinements as well. Showing the independence of stability constants upon order p, however, remains an open question.

The concept and name of the *Discontinuous Petrov Galerkin* (DPG) method were introduced by Bottasso, Micheletti, Sacco and Causin in [6, 7, 8, 9]. The critical idea of optimal test functions computed on a fly was introduced by Demkowicz and Gopalakrishnan in [14, 15, 16].

The main promise of the DPG method with optimal test functions is that it guarantees discrete stability, if the underlying continuous problem is well-posed. The method delivers the best approximation in a problem-dependent energy (residual) norm [14, 15, 16]. Moreover, with an appropriate choice of norm for the test space, one can deliver the best approximation in a norm of choice, starting with the L^2-norm [30, 21].

This report is devoted to a numerical comparison and illustration of the two methods using 2D examples. After a short description of both methodologies in Section 2 and in Section 3, the bulk of the paper is devoted to numerical experiments presented in Section 4. We conclude with a brief discussion in Section 5.

2 Dual–Mixed Elasticity with Weakly Imposed Symmetry

We start with a system of first order equations,

$$\begin{cases} C_{ijkl}\sigma_{kl} - u_{i,j} + \omega_{ij} = 0 & i,j = 1,2,3 \\ \sigma_{ij,j} = f_i & i = 1,2,3 \\ \sigma_{ij} - \sigma_{ji} = 0 & i,j = 1,2,3 \end{cases} \tag{2.1}$$

Here C_{ijkl} is the compliance tensor, σ_{kl} is the stress tensor, u_i is the displacement vector, $\omega_{ij} = (u_{i,j} - u_{j,i})/2$ denotes the tensor of infinitesimal rotation, and f_i stands for the body force. The first set of equations combines Hooke's constitutive law with Cauchy's geometrical relations, the second set represents conservation of linear momentum which reduces to the equilibrium equations in the static case, and the last set, the symmetry of stress tensor, is a consequence of conservation of angular momentum.

The system is to be solved in a bounded domain Ω, and it is accompanied with kinematic boundary conditions on Γ_u, and traction boundary conditions on Γ_t, where $\Gamma_u \cup \Gamma_r = \partial\Omega$,

$$u_i = \bar{u}_i \text{ on } \Gamma_u \quad \text{and} \quad t_i := \sigma_{ij} n_j = \bar{t}_i \text{ on } \Gamma_t \tag{2.2}$$

We use the Einstein summation convention, and n_i is the outward normal unit vector on $\partial\Omega$.

In order to derive the variational formulation, we multiply the first equation with a test tensor τ_{ij}, integrate over the domain, and integrate the second term by parts to obtain,

$$\int_\Omega C_{ijkl}\sigma_{kl}\tau_{ij} + \int_\Omega u_i \tau_{ij,j} - \int_{\partial\Omega} u_i \tau_{ij} n_j + \int_\Omega \omega_{ij}\tau_{ij} = 0 \tag{2.3}$$

Next, we build into the variational equation the kinematic boundary conditions replacing u_i in the boundary term with the known data,

$$\int_\Omega C_{ijkl}\sigma_{kl}\tau_{ij} + \int_\Omega u_i \tau_{ij,j} + \int_\Omega \omega_{ij}\tau_{ij} = \int_{\partial\Omega} \bar{u}_i \tau_{ij} n_j \tag{2.4}$$

The second and third equations are treated differently. We multiply the equilibrium equations with a test function v_i, and integrate it over Ω, but we do not relax it, i.e. we do not integrate by parts. The third equation is an algebraic equation only, we satisfy it by requesting the L^2-orthogonality of the stress tensor with antisymmetric test tensors w_{ij}. The final variational formulation reads as follows,

$$\left\{\begin{array}{l} \sigma \in H(\mathrm{div},\Omega;\mathbb{M}), \sigma_{ij}n_j = \bar{t}_i \text{ on } \Gamma_t,\ u \in L^2(\Omega;\mathbb{V}),\ \omega \in L^2(\Omega;\mathbb{K}), \omega_{ij} = \omega_{ji} \\ \begin{array}{llll} \displaystyle\int_\Omega C_{ijkl}\sigma_{kl}\tau_{ij} & + \displaystyle\int_\Omega u_i\tau_{ij,j} & + \displaystyle\int_\Omega \omega_{ij}\tau_{ij} & = \displaystyle\int_{\partial\Omega} \bar{u}_i\tau_{ij}n_j \quad \tau \in H(\mathrm{div},\Omega;\mathbb{M}) \\ -\displaystyle\int_\Omega \sigma_{ij,j}v_i & & & = \displaystyle\int_\Omega f_i v_i \qquad v \in L^2(\Omega;\mathbb{V}) \\ \displaystyle\int_\Omega \sigma_{ij}w_{ij} & & & = 0 \qquad\qquad w_{ij} = -w_{ji} \in L^2(\Omega;\mathbb{K}) \end{array} \end{array}\right. \tag{2.5}$$

Here $\mathbb{M}, \mathbb{V}, \mathbb{K}$ denote the space of second order tensors, the space of vectors, and the space of antisymmetric tensors, respectively. The symbol $H(\mathrm{div},\Omega;\mathbb{M})$ denotes fields with values in $\mathbb{M}$, that are square integrable along with their divergence computed row-wise, and $L^2(\Omega;\mathbb{V})$ and $L^2(\Omega;\mathbb{K})$ stand for the square integrable fields with values in $\mathbb{V}, \mathbb{K}$, respectively. The formulation clearly falls within the Brezzi's theory for mixed problems.

Discretization is based on tetrahedral elements and Nédélec's spaces of the second kind forming the discrete exact sequence,

$$\mathcal{P}_{p+3}\Lambda^0(\mathcal{T}_h) \xrightarrow{\text{grad}} \mathcal{P}_{p+2}\Lambda^1(\mathcal{T}_h) \xrightarrow{\text{curl}} \mathcal{P}_{p+1}\Lambda^2(\mathcal{T}_h) \xrightarrow{\text{div}} \mathcal{P}_p\Lambda^3(\mathcal{T}_h) \tag{2.6}$$

where $\mathcal{T}_h$ stands for a tetrahedral mesh, and the exponent k in Λ^k denotes the global conformity type: $H^1, H(\mathrm{curl}), H(\mathrm{div})$ and L^2-conforming elements for $k = 0, 1, 2, 3$, respectively. The discretization is actually based only on the last two spaces in the sequence, rows of the stress tensor are discretized with polynomials from $\mathcal{P}_{p+1}\Lambda^2(\mathcal{T}_h)$, and components of both the displacement vector and infinitesimal rotation come from $\mathcal{P}_p\Lambda^3(\mathcal{T}_h)$. We use the differential forms notation; note that the first and last space in the sequence consists of scalar-valued fields, whereas the second and third includes vector-valued fields.

Discrete stability. Even though the computations are done with elements of the second type only, the proof of Brezzi's conditions involves also the last three spaces in the exact sequence for Nédélec's elements of the first type,

$$\mathcal{P}_{p+1}\Lambda^0(\mathcal{T}_h) \xrightarrow{\text{grad}} \mathcal{P}^-_{p+1}\Lambda^1(\mathcal{T}_h) \xrightarrow{\text{curl}} \mathcal{P}^-_{p+1}\Lambda^2(\mathcal{T}_h) \xrightarrow{\text{div}} \mathcal{P}_p\Lambda^3(\mathcal{T}_h) \tag{2.7}$$

where

$$\begin{aligned}\mathcal{P}_p^-(T;\mathbb{V}) &:= \mathcal{P}_{p-1}(T;\mathbb{V}) + \boldsymbol{x}\times\mathcal{P}_{p-1}(T;\mathbb{V})\\ \mathcal{P}_p^-(T;\mathbb{V}) &:= \mathcal{P}_{p-1}(T;\mathbb{V}) + \boldsymbol{x}\mathcal{P}_{p-1}(T)\end{aligned} \tag{2.8}$$

with T denoting a single tetrahedron.

In the proof of stability, the following three commuting diagrams turn out to be essential.

$$\begin{array}{ccc} H^1(\Omega;\mathbb{M}) & \xrightarrow{\text{div}} & L^2(\Omega;\mathbb{V}) \\ \Pi^2_{p,h}\downarrow & & \Pi^3_{p,h}\downarrow \\ \mathcal{P}_{p+1}\Lambda^2(\mathcal{T}_h;\mathbb{V}) & \xrightarrow{\text{div}} & \mathcal{P}_p\Lambda^3(\mathcal{T}_h;\mathbb{V}) \end{array} \tag{2.9}$$

$$\begin{array}{ccc} H^1(\Omega;\mathbb{M}) & \xrightarrow{\text{div}} & L^2(\Omega;\mathbb{V}) \\ \Pi^{2,-}_{p,h}\downarrow & & \Pi^3_{p,h}\downarrow \\ \mathcal{P}^-_{p+1}\Lambda^2(\mathcal{T}_h;\mathbb{V}) & \xrightarrow{\Pi^3_{p,h}\circ\text{div}} & \mathcal{P}_p\Lambda^3(\mathcal{T}_h;\mathbb{V}) \end{array} \tag{2.10}$$

$$\begin{array}{ccc} H^1(\Omega;\mathbb{M}) & \xrightarrow{S_1} & H^1(\Omega;\mathbb{M}) \\ \overline{\Pi}^{1,-}_{p,h}\downarrow & & \Pi^{2,-}_{p,h}\downarrow \\ \mathcal{P}^-_{p+2}\Lambda^1(\mathcal{T}_h;\mathbb{V}) & \xrightarrow{\Pi^{2,-}_{p,h}\circ S_1} & \mathcal{P}^-_{p+1}\Lambda^2(\mathcal{T}_h;\mathbb{V}) \end{array} \tag{2.11}$$

Notation may be a bit confusing. E.g., presence of symbol $\mathbb{V}$ in $\mathcal{P}^-_{p+1}\Lambda^2(\mathcal{T}_h;\mathbb{V})$ indicates that we take three copies of already vector-valued fields, hence the space is isomorphic with tensor-valued fields. Above, $\Pi^3_{p,h}$ is the L^2 orthogonal projection operator onto $\mathcal{P}_p\Lambda^3(\mathcal{T}_h;\mathbb{V})$, $\Pi^2_{p,h}$, $\Pi^{2,-}_{p,h}$, and $\overline{\Pi}^{1,-}_{p,h}$ are projection operators into $\mathcal{P}_{p+1}\Lambda^2(\mathcal{T}_h;\mathbb{V})$, $\mathcal{P}^-_{p+1}\Lambda^2(\mathcal{T}_h;\mathbb{V})$, and $\mathcal{P}^-_{p+2}\Lambda^1(\mathcal{T}_h;\mathbb{V})$ respectively, and S_1 denotes an algebraic operator,

$$S_1 W = W^\top - \text{tr}(W)I \tag{2.12}$$

For an arbitrary but uniform polynomial order p, canonical projection operators have been used in [4, 5, 18] to make diagrams (2.9),(2.10),(2.11) simultaneously commute.

Stability proof for elements of variable order. Although the generalization of the involved polynomial spaces to elements of variable order is rather straightforward [12, 17], an attempt to generalize the stability proof of Arnold, Falk and Winther, turned to be challenging.

Canonical projection operators used in diagrams (2.9) and (2.9) fail to commute for elements of variable order, see a counterexample in [22]. Our first attempt was based on replacing the canonical interpolation operators with Projection-Based (PB) interpolation operators [13] that not only commute on elements of variable order but also yield optimal p-convergence estimates. Then, however, we need to construct a special

operator $\overline{\Pi}_h^{1,-}$ to make diagram (2.11) commute as well. In [22], we use the very commutativity property to design an operator $\overline{\Pi}_h^{1,-}$ (denoted in [22] by $\widetilde{W}_h$) that makes the diagram commute. With the commuting property in place, the difficulty shifted to proving that the operator is well-defined. Although 2D numerical experiments indicated the non-singularity of the operator for $p = 1, \ldots, 15$, we were able to prove it only for two space dimensions, and rather limited order of approximation: $p = 0, 1, 2, 3$, see [22].

A new idea has been presented in [23, 24]. Instead of constructing operators $\Pi_h^{2,-}$ and $\overline{\Pi}_h^{1,-}$ explicitly, we only show their existence. This is done by introducing a one-parameter family of PB-like operators $\Pi_{T,t}^{2,-}$ onto $\mathcal{P}_{p+1}^{-}\Lambda^2(\mathcal{T}_h;\mathbb{V})$, and a corresponding one-parameter family of operators $\overline{\Pi}_{T,t}^{1,-}$ into $\mathcal{P}_{p+2}^{-}\Lambda^1(\mathcal{T}_h;\mathbb{V})$, with $t \in [0,1]$. We design $\Pi_{T,t}^{2,-}$ and $\overline{\Pi}_{T,t}^{1,-}$ in such a way that $\Pi_{T,0}^{2,-}$ coincides with the original PB operator $\Pi_h^{2,-}$ (and, therefore, it is well-defined) and that we can show that $\overline{\Pi}_{T,1}^{1,-}$ is well-defined as well. The non-singularity of both operators translates into non-zero determinants of the corresponding matrix representations with respect to specific bases. Both determinants are polynomials in t and, since they are non-zero at $t = 0$ or $t = 1$, there must not not be identically zero. By the Fundamental Theorem of Algebra, the determinants can have only a finite number of roots. This proves that both operators are well-defined for $t \in [0,1]$, except for a finite number of values. In addition, we design $\Pi_{T,t}^{2,-}$ and $\overline{\Pi}_{T,t}^{1,-}$ in such a way that the 'pull back' of them on the reference element $\hat{T}$ is independent of T, so the choice of parameter t is done on the master element, and it is independent of a particular element T.

Using the reasoning of Arnold, Falk and Winther, we used the three commuting diagrams to prove the mesh independence of stability constants for elements of variable but limited order (the constants do depend upon the maximum order in the mesh).

The proof of stability for the p- and hp versions of the method remains open.

3 Discontinuous Petrov Galerkin Method

We start with the same system of first order equations as for the dual-mixed method,

$$\begin{cases} C_{ijkl}\sigma_{kl} - u_{i,j} + \omega_{ij} = 0 & i,j = 1,2,3 \\ \sigma_{ij,j} = f_i & i = 1,2,3 \end{cases} \tag{3.13}$$

Here C_{ijkl} is the compliance tensor, σ_{kl} is the stress tensor, u_i is the displacement vector, $\omega_{ij} = (u_{i,j} - u_{j,i})/2$ denotes the tensor of infinitesimal rotation, and f_i stands for the body force. We shall assume from start that the stress tensor is symmetric, $\sigma_{ij} = \sigma_{ji}$.

Given an arbitrary element K, we multiply the first equation with q_j, integrate over the element, and integrate the second term by parts to obtain:

$$\int_K C_{ijkl}\sigma_{kl}q_j + \int_K u_i q_{j,j} - \int_{\partial K} u_i \underbrace{q_j n_j}_{=:q_{n_K}} + \int_K \omega_{ij}q_j = 0, \quad i = 1,2,3 \tag{3.14}$$

The resulting flux u_i is declared to be an independent unknown, and will be denoted with a "hat" symbol, $\hat{u}_i$. The element outward unit vector is denoted by n_K, and q_{n_K} stands for the outward normal component of the vector-valued testing function q_j. Had we tested with a *symmetric* tensor $\tau_{ij} = \tau_{ji}$, the infinitesimal rotations ω_{ij} would have been eliminated. The reason we test with less restrictive test functions is the same as in the mixed method, the resulting energy space for q_j, $H(\text{div}, K)$, is easier to discretize.

Contrary to the mixed method, we do not assume a global conformity for testing functions q_j, i.e. they live in the "broken" $H(\text{div})$ space only. Testing with globally conforming test functions eliminates the fluxes from the formulation but does not allow to pursue the concept of optimal test functions to be discussed in a moment.

We continue in the same way with the second equation. We multiply the second equation with a *scalar-valued* test function v, integrate over element K, and integrate by parts to obtain:

$$\int_K \sigma_{ij} v_{,j} - \int_{\partial K} \sigma_{ij} n_j v = \int_K f_i v \tag{3.15}$$

Notice that, in the mixed method, the equation remains in the strong form, i.e. it is *not* integrated by parts. With each element face (edge in 2D), we identify now one of two possible normals for the face, in other words, we assume that the face comes with a predefined orientation n^F. The traction $t_i = \sigma_{ij} n_j^F$ is assumed again to be an independent unknown (flux) and will be denoted with $\hat{t}_i$. With the flux in place, the equation reads as follows,

$$\int_K \sigma_{ij} v_{,j} - \int_{\partial K} \hat{t}_i \text{sgn}(n_K) v = \int_K f_i v \tag{3.16}$$

where

$$\text{sgn}(n_K) = \begin{cases} 1 & \text{if } n_K = n_K^F \\ -1 & \text{if } n_K = -n_K^F \end{cases} \tag{3.17}$$

On the boundary of the domain, the fluxes match the known data:

$$\hat{u}_i = \bar{u}_i \text{ on } \Gamma_u \quad \text{and} \quad \hat{t}_i = \bar{t}_i \text{ on } \Gamma_t \tag{3.18}$$

Here Γ_u and Γ_t denote the two disjoint parts of boundary $\partial\Omega$ where the kinematic $\bar{u}_i$ and traction $\bar{t}_i$ boundary data are specified. Notice that $\bar{t}_i$ do not necessary correspond to the outward normal unit vector but to the prespecified vector n^F orienting the boundary faces (edges). Vector n^F may coincide with the outward or inward unit vector, depending upon the face (edge) orientations.

The final variational formulation reads as follows.

$$\begin{cases} \sigma_{ij}, u_i, \omega_{ij} \in L^2(\Omega),\ \sigma_{ij} = \sigma_{ji},\ \omega_{ij} = -\omega_{ji} & \\ \hat{u}_i \in H^{\frac{1}{2}}(\Gamma), \hat{t}_i \in H^{-\frac{1}{2}}(\Gamma) & \\ \hat{u}_i = \bar{u}_i & \text{on } \Gamma_u \\ \hat{t}_i = \bar{t}_i & \text{on } \Gamma_t \\ \displaystyle\int_K C_{ijkl}\sigma_{kl} q_j + \int_K u_i q_{j,j} - \int_{\partial K} \hat{u}_i q_{n_K} + \int_K \omega_{ij} q_j = 0, & i = 1,2,3,\ q \in H(\text{div}, K) \\ \displaystyle\int_K \sigma_{ij} v_{,j} - \int_{\partial K} \hat{t}_i \text{sgn}(n_K) v = \int_K f_i v & i = 1,2,3,\ v \in H^1(K) \end{cases} \tag{3.19}$$

for every element K in the mesh. Above, Γ stands for the union of all element faces (edges), $H^{\frac{1}{2}}(\Gamma)$ is the space of traces of functions from $H^1(\Omega)$ to Γ,

$$H^{\frac{1}{2}}(\Gamma) := \{u|_\Gamma \ : \ u \in H^1(\Omega)\} \tag{3.20}$$

and the definition of space $H^{-\frac{1}{2}}(\Gamma)$ is more technical. Functionals from $H^{-\frac{1}{2}}(\Gamma)$ must be well-defined when applied to test functions $v \in H^1(K)$, for individual elements K, and they must be single-valued on the interelement boundary. We will not enter the technical discussion here and assume only that such energy space exists and is well-defined.

The variational formulation can be written in the usual abstract form,

$$\begin{cases} u \in U \\ \\ b(u,v) = l(v), \quad v \in V \end{cases} \tag{3.21}$$

where u denotes the group variable $u = (\sigma_{ij}, u_i, \omega_{ij}, \hat{u}_i, \hat{t}_i)$, and $v = (q^i, v^i)$ the group test function consisting of three $H(\text{div})$-conforming test functions q^i, and three H^1-conforming test functions v^i. The number of test functions matches the number of field unknowns. To complete the variational formulation, we need to specify a norm for the test functions. We shall consider two test norms. The first one is a standard combination of $H(\text{div})$ and H^1 norms,

$$\|v\|^2 = \sum_{i=1}^{3} \int_K \{|\text{div} q^i|^2 + |q^i|^2\} + \sum_{i=1}^{3} \int_K \{|\nabla v^i|^2 + |v^i|^2\} \tag{3.22}$$

The upper indices for test functions indicate the three copies of $H(\text{div})$-conforming, and the three copies of H^1-conforming test functions.

The second norm is implied by the problem and corresponds to an optimal test norm defined abstractly by:

$$\|v\| = \sup_{\|u\|=1} |b(u,v)| \tag{3.23}$$

In order to derive the norm, we first rewrite variational form (3.19) in an equivalent form,

$$\begin{cases} \displaystyle\int_K C_{ijkl}\sigma_{kl} q^i_j + \int_K u_i q^i_{j,j} - \int_{\partial K} \hat{u}_i q^i_{n_K} + \int_K \omega_{ij} q^i_j &= 0 \\ \\ \displaystyle\int_K \sigma_{ij} v^i_{,j} - \int_{\partial K} \hat{t}_i \text{sgn}(n_K) v^i &= \displaystyle\int_K f_i v^i \end{cases} \tag{3.24}$$

Summing over all elements K, regrouping the terms, and factoring out the unknown field variables and fluxes, we obtain an equivalent formula for the global bilinear form,

$$b(u,v) = \sum_K \int_K \{(C_{ijkl} q^i_j + v^k_{,l})\sigma_{kl} + q^i_{j,j} u_i + q^i_j \omega_{ij}\} + \sum_e \int_e \{[q^i_n]\hat{u}_i + [v^i]\hat{t}_i\} \tag{3.25}$$

where $q^i_{n_K} = \text{sgn}(n_K) q^i_n$, brackets denote jumps of test functions across the interelement boundaries, and the second sum corresponds to all edges e in the mesh.

Symmetry of the stress tensor implies that

$$(C_{ijkl}q^i_j + v^k_{,l})\sigma_{kl} = \{C_{ijkl}q^i_j + v^k_{,l}\}_s\sigma_{kl} \tag{3.26}$$

where $\{\cdot\}_s$ denotes the symmetric part of the tensor. Similarly, antisymmetry of ω_{ij} implies that

$$q^i_j\omega_{ij} = \{q^i_j\}_a\omega_{ij} \tag{3.27}$$

where $\{\cdot\}_a$ denotes the antisymmetric part of the tensor. Taking supremum with respect to the field variables and fluxes, we obtain the final formula:

$$\begin{aligned}\|v\|^2 &= \sum_{k=1}^{3}\sum_{l=1}^{3}\|\{C_{ijkl}q^i_j + v^k_{,l}\}_s\|^2_{L^2(\Omega)} + \sum_{i=1}^{3}\|q^i_{j,j}\|^2_{L^2(\Omega)} + \sum_{k=1}^{3}\sum_{l=1}^{3}\|\{q^i_j\}_a\|^2_{L^2(\Omega)} \\ &+ \sum_{i=1}^{3}\|[q^i_n]\|^2_? + \|[v^i]\|^2_?\end{aligned} \tag{3.28}$$

The norms on the jumps are implied by the choice of norm for the fluxes. This is, of course, a purely formal result. Proving that the expression above is indeed a norm equivalent to the first one is equivalent to showing the inf-sup condition for the bilinear form, i.e. proving that the variational formulation is well posed.

Our second norm is going to be a modification of the optimal norm (3.28). We simply replace the jump terms with L^2-norms for the individual components of the test functions premultiplied with a coefficient β,

$$\begin{aligned}\|v\|^2 &= \sum_{k=1}^{3}\sum_{l=1}^{3}\|\{C_{ijkl}q^i_j + v^k_{,l}\}_s\|^2_{L^2(\Omega)} + \sum_{i=1}^{3}\|q^i_{j,j}\|^2_{L^2(\Omega)} + \sum_{k=1}^{3}\sum_{l=1}^{3}\|\{q^i_j\}_a\|^2_{L^2(\Omega)} \\ &+ \beta\sum_{i=1}^{3}\{\|q^i\|^2_{L^2(\Omega)} + \|v^i\|^2_{L^2(\Omega)}\}\end{aligned} \tag{3.29}$$

Discretization. We restrict now ourselves to the 2D case only. In 2D, antisymmetric tensor ω_{ij} reduces to a single unknown,

$$\omega_{ij} = \begin{pmatrix} 0 & p \\ -p & 0 \end{pmatrix} \tag{3.30}$$

All field unknowns $\sigma_x, \tau_{xy}, \sigma_y, u, v, p$ will be discretized with standard L^2-conforming elements [1] corresponding to spaces $\mathcal{P}^p(\hat{K})$ on a master triangle $\hat{K}$, and tensor products $\mathcal{P}^p(\hat{I}) \otimes \mathcal{P}^q(\hat{I})$, for a master unit square $\hat{K} = \hat{I}^2$. In our implementation, we have complied with the definition of parametric elements and Piola transforms, see e.g. [12], page 308. The fluxes are discretized with one-dimensional L^2-conforming elements or order $p_f + \Delta p_f$ corresponding to element edges. The order for elements may vary locally, with the possible anisotropic order for quads. The flux order p_f is determined using the *maximum rule*, i.e. for a given edge e, it is set to the maximum order of all elements adjacent to the edge (accounting for directionality in the case of quads). Symbol Δp_f denotes an increment (uniform for the whole mesh) that

[1] We hope to survive the notational collision between infinitesimal rotation component p and polynomial order of approximation p.

may be both positive and negative. Introducing Δp_f into the code allows for studying the relation between the discretization for field variables and fluxes. We enforce 1-irregularity of meshes during h-refinements. In the case of a "big" element sharing an edge with two small neighbors, we discretize the flux using the smaller edges, i.e. the flux is *piecewise polynomial* on the big edge with the order p_f set to the maximum order of neighboring elements.

Notice that we commit a "variational crime" in discretizing fluxes [2] $u, v \in H^{\frac{1}{2}}(\Gamma)$, the discretization is non-conforming. We hope that this ϵ-crime will be forgiven. Implementation of an H^1-conforming discretization for fluxes u, v would have resulted in larger stencils (elements would communicate through vertices as well) and complicated the implementation.

Fluxes corresponding to boundary conditions are determined by performing L^2-projections of the data. The corresponding boundary integrals in the variational formulation are moved to the right-hand side, contributing to the load vector. This is in full analogy to the implementation of Dirichlet boundary conditions for standard conforming discretizations. As the discretization is L^2-conforming only, there is no need for constrained approximation (hanging nodes) in the implementation.

Optimal test functions. Trial functions are scalar-valued. For each trial function u, approximating one of the field variables or one of the fluxes, we determine the corresponding vector-valued *optimal test function* by solving a variational problem:

$$\begin{cases} v \in V \\ (v, \delta v) = b(u, \delta v), \quad \delta v \in V \end{cases} \tag{3.31}$$

Here $(\cdot, \cdot)$ denotes the inner product corresponding to one of the test norms [3], and V is the test space. Due to the fact that the test functions are discontinuous, and that both norms (3.22) and (3.29) can be represented as sums of element contributions defining norms over individual elements [4], the optimal test functions can be determined element-wise by solving local variational problems defined over elements:

$$\begin{cases} v \in V(K) \\ (v, \delta v)_K = b(u, \delta v), \quad \delta v \in V(K) \end{cases} \tag{3.32}$$

In the case of a trial function corresponding to one of the field variables, with a support in element K, the optimal test function is supported over the same element K as well. In the case of a flux trial function that "lives" on edge e, the corresponding optimal test function spans over the two (one if the edge is on the boundary of the domain) elements sharing the edge. Each of the two element contributions is computed locally, one element at a time.

The local variational problems defining the optimal test functions are approximated by replacing the test space with a discrete *enriched space*. In the reported experiments, we have used standard $H(\mathrm{div})$- and

[2] Some colleagues call them "traces".
[3] We work with Hilbert spaces only.
[4] We call them *localizable norms*.

H^1-conforming elements increasing the local, element order of approximation from p to $p+\Delta p$ (for quads: $(p+\Delta p, q+\Delta p)$) where Δp is a global parameter. The enriched space *should not be confused* with the (optimal) test space that is defined as the span of element test functions. The test space forms only a proper subspace of the enriched space.

Computation of the optimal test functions does not alter the usual FE algorithms, as all additional computations are done on the element level.

We record now the main points about the method, see [15, 16, 30] for a detailed discussion.

- The optimal test functions realize the supremum in the inf-sup condition.
- Neglecting the error due to approximation of optimal test functions, the DPG method delivers the *best approximation error* in the problem–dependent energy (residual) norm,

$$\|u\|_E := \sup_{\|v\|_V=1} |b(u,v)| \tag{3.33}$$

- With norm (3.29) in use, we expect the energy norm to be close to the L^2-norm for the field variables.
- The stiffness matrix is symmetric and positive-definite. Indeed, the method can be interpreted as a least-squares method in an appropriate norm.
- There is no need for an a-posteriori error estimation. The discretization error can be computed by solving local problems,

$$\begin{cases} v_e \in V(K) \\ (v_e, \delta v)_K = b(u_{hp}, \delta v) - l(\delta v), \quad \delta v \in V(K) \end{cases} \tag{3.34}$$

  and summing the element contributions:

$$\|u_{hp} - u\|_E^2 = \sum_K \|v_e\|_{V(K)}^2 \tag{3.35}$$

  Here u_{hp} denotes an approximate solution, and v_e is called the *error representation function*. Similarly to the optimal test functions, the error representation function is approximated by solving the local problem approximately in the enriched space.

4 Numerical experiments

In this section we present numerical results for two simple model problems: a rectangular plate problem and the L-shape domain problem. Solutions to both problems are singular. The L-shape domain problem is used to compare the AFW and DPG methods.

4.1 Rectangular plate problem

We consider a plate occupying a unit square domain with the left edge fixed, and pulled with a uniform horizontal traction along the right edge, see Fig. 1. Due to the change of boundary conditions, we expect singularities in stresses at top-left and bottom-left corners of the plate.

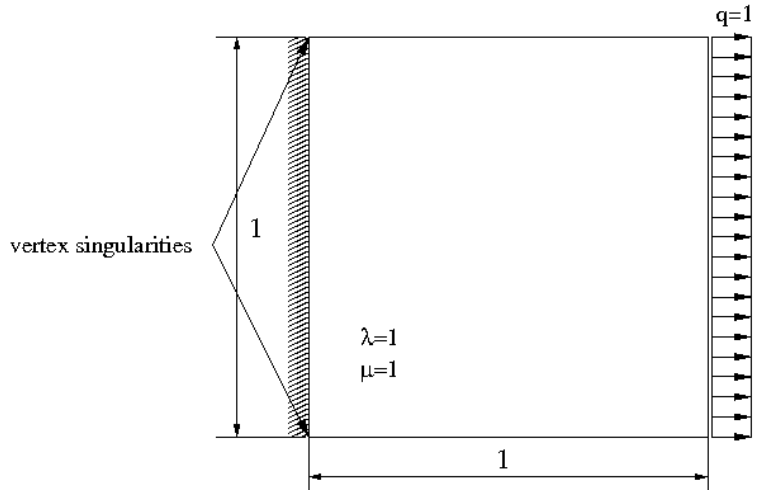

Figure 1: Rectangular plate problem data.

We do not know the exact solution to the problem, and we can only verify expected convergence rates. The problem has been solved using the standard test norm (3.22) and three adaptive strategies: uniform h, h-adaptive, and hp-adaptive refinements. We start with a mesh of four biquadratic elements ($p = 2$), use $\Delta p = 3$ for the enriched spaces, and $\Delta p_f = 1$ for fluxes, i.e. the order for fluxes is one order higher than for the field variables. For h-refinements, we use the energy error (3.35) and the standard "greedy strategy", i.e. in each step we refine all elements whose contributions are within γ percent of the maximum element contribution. In all reported computations, we use $\gamma = 0.49$. For the hp-refinements, we use the Ainsworth marking strategy. We mark singular vertices and, if an element chosen for a refinement contains a singular vertex, it is h-refined, otherwise, it is p-refined. Finally, we take advantage of quad elements and allow for anisotropic refinements. We use an ad-hoc anisotropy indicator based on the error representation function. We split the element error contributions into three terms:

$$\begin{aligned} \text{derror}_1 &= \sum_{i=1}^{3} \int_K \{|\text{div} q^j|^2 + |v^j|^2\} \\ \text{derror}_2 &= \sum_{i=1}^{3} \int_K \{|q_1^j|^2 + |\frac{\partial v^j}{\partial x_1}|^2\} \\ \text{derror}_3 &= \sum_{i=1}^{3} \int_K \{|q_2^j|^2 + |\frac{\partial v^j}{\partial x_2}|^2\} \end{aligned} \tag{4.36}$$

If $0.1 * \text{derror}_2 \geq \text{derror}_3$, we refine the element in the direction of x_1-axis, i.e. we either break it across the x_1-axis or increase the polynomial order in that direction. We proceed analogously, if $0.1 * \text{derror}_3 \geq \text{derror}_2$.

Fig. 2 displays the convergence history for the three types of refinements. As expected, h-adaptivity has restored the optimal rate of convergence for the L^2-norm. Note that in 2D, number N of d.o.f. is proportional to h^{-2}, so the rate h^3 translates into $N^{-\frac{3}{2}}$. Fig. 3 shows the optimal hp mesh after 15 refinements, and the

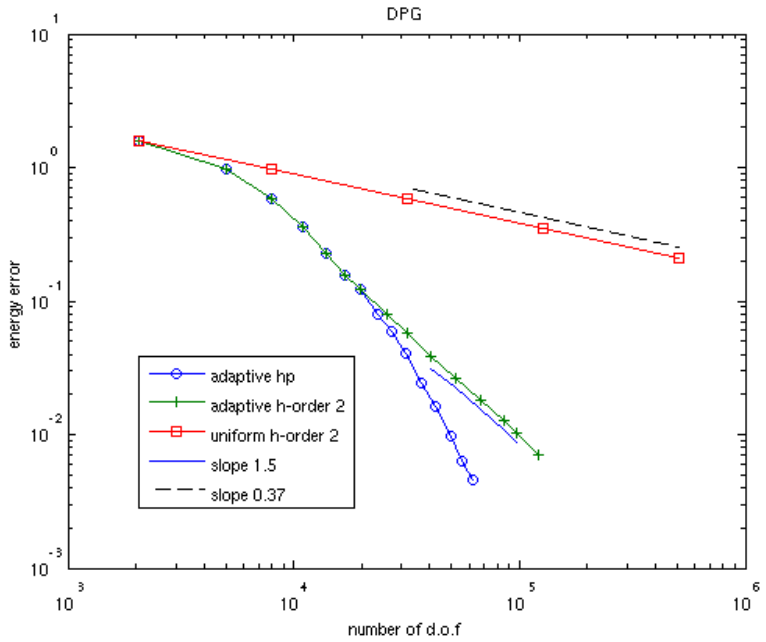

Figure 2: Plate problem. Convergence history for uniform, h-adaptive and hp-adaptive refinements. Energy norm of the error vs. number of d.o.f.

corresponding distribution of σ_x. The contour map shows no trace of mesh which is evidence of a resolved solution. The displayed range is between 0.85 and 1.15. The stress matches the imposed traction along the east edge and exhibits strong singularities at the corners where the displacement and traction boundaries meet. The maximum values of the stress at the singular corners is of order 10, a numerical "equivalent" of ∞. Decreasing order for fluxes, i.e. for $\Delta p_f = 0$, we get the same convergence rates for the uniform h-refinements, but we loose the optimal rate of convergence for the h-adaptive refinements. This is illustrated in Fig. 4.

4.2 L-shape domain problem

We choose for domain the standard L-shape domain shown in Fig 5. We assume homogeneous kinematic boundary conditions along the reentrant edges $x_1 = 0$ and $x_2 = 0$, and non-homogeneous traction boundary conditions along the rest of the boundary. We shall use a manufactured solution corresponding to the exact

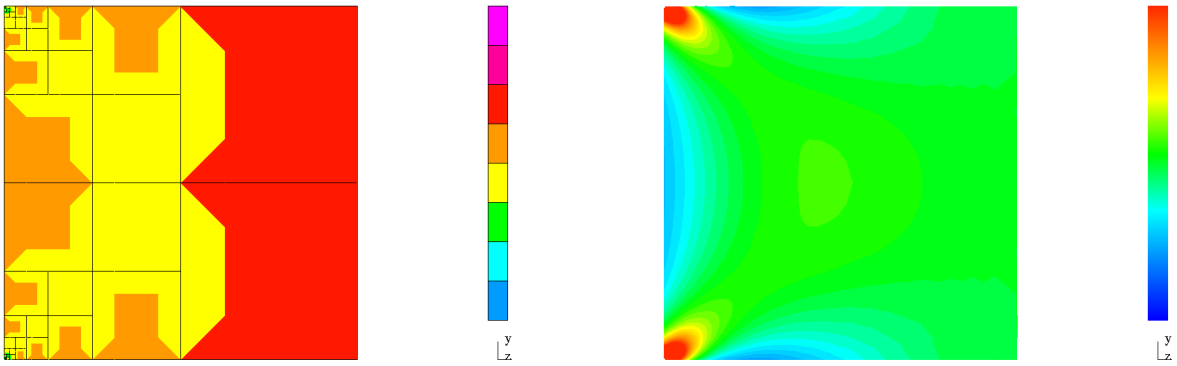

Figure 3: Plate problem. Optimal hp mesh after 15 refinements and the corresponding distribution of σ_x.

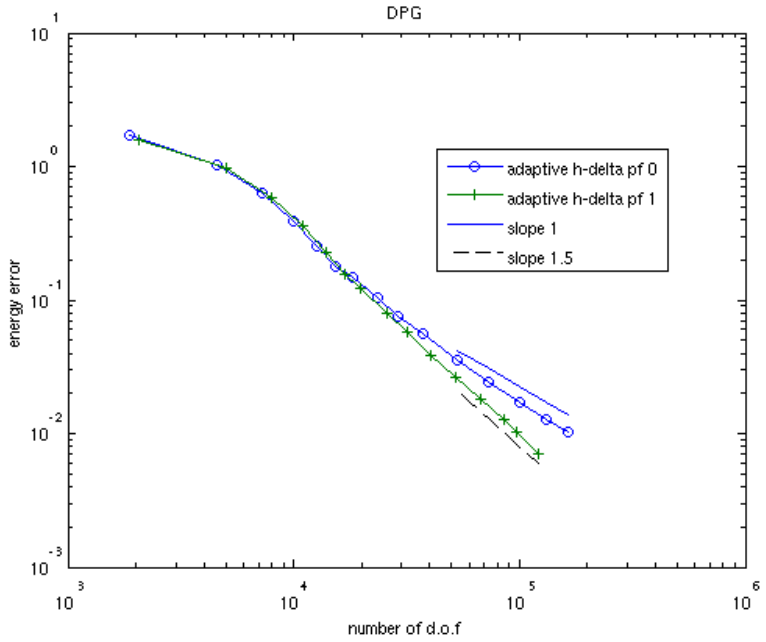

Figure 4: Plate problem. Convergence history for h-adaptive refinements using $\Delta p_f = 1$ and $\Delta p_f = 0$. Decreasing the order for fluxes results in a loss of the optimal convergence rate.

solution of the homogeneous equilibrium equations (zero body forces), and the corresponding unbounded L-shape domain extending to infinity. Following the Airy stress function approach presented in [29], we arrive at the following formulas for stresses and displacements in the system of polar coordinates r, θ. Notice that angle θ is measured from line $x_1 = x_2$, see Fig. 5.

The stresses are expressed as:

$$\sigma_r = r^{a-1}\left[F''(\theta) + (a+1)F(\theta)\right]$$
$$\sigma_\theta = a(a+1)r^{a-1}F(\theta)$$
$$\sigma_{r\theta} = -ar^{a-1}F'(\theta)$$

with the displacements expressed by:

$$u_r = \frac{1}{2\mu}r^a\left[-(a+1)F(\theta) + \left(1 - \frac{\nu}{1+\nu}\right)G'(\theta)\right]$$
$$u_\theta = \frac{1}{2\mu}r^a\left[-F'(\theta) + \left(1 - \frac{\nu}{1+\nu}\right)(a-1)G(\theta)\right]$$

Here $\nu = \frac{\lambda}{2(\lambda+\mu)}$ is the Poisson ratio. Functions $F(\theta)$ and $G(\theta)$ have the form

$$F(\theta) = C_1\sin(a+1)\theta + C_2\cos(a+1)\theta + C_3\sin(a-1)\theta + C_4\cos(a-1)\theta,$$
$$G(\theta) = \frac{4}{a-1}\left[-C_3\cos(a-1)\theta + C_4\sin(a-1)\theta\right]$$

where constants C_1, C_2, C_3, C_4 and a, are to be determined from kinematic boundary conditions and energy considerations. One can verify that the stresses are divergence free, $\mathrm{div}\sigma = 0$ and, therefore, satisfy the equilibrium equations with zero body forces. One can also verify that the strain tensor corresponding to the displacements, and the stress tensor satisfy the Hooke's law.

The kinematic boundary conditions lead to equations:

$$-(a+1)F(\theta) + \left(1 - \frac{\nu}{1+\nu}\right)G'(\theta) = 0,$$
$$-F'(\theta) + \left(1 - \frac{\nu}{1+\nu}\right)(a-1)G(\theta) = 0$$

to be satisfied at $\theta = \pm\frac{3}{4}\pi$. This leads to the following relations for the constants C_1, C_2, C_3, C_4,

$$\frac{C_1}{C_3} = \frac{\left[4\left(1 - \frac{\nu}{1+\nu}\right) - (a+1)\right]\sin(a-1)\frac{3}{4}\pi}{(a+1)\sin(a+1)\frac{3}{4}\pi}$$
$$= \frac{-\left[4\left(1 - \frac{\nu}{1+\nu}\right) + (a-1)\right]\cos(a-1)\frac{3}{4}\pi}{(a+1)\cos(a+1)\frac{3}{4}\pi},$$

or

$$\frac{C_2}{C_4} = \frac{\left[4\left(1 - \frac{\nu}{1+\nu}\right) - (a+1)\right]\cos(a-1)\frac{3}{4}\pi}{(a+1)\cos(a+1)\frac{3}{4}\pi}$$
$$= \frac{-\left[4\left(1 - \frac{\nu}{1+\nu}\right) + (a-1)\right]\sin(a-1)\frac{3}{4}\pi}{(a+1)\sin(a+1)\frac{3}{4}\pi}.$$

For material constants $\lambda = 99.3$, $\mu = 66.1638$, the smallest $a < 1$ for which the stress is still square integrable corresponds to the choice $C_2 = C_4 = 0$ and equals $a = 0.60404$. We choose $C_3 = 1$, and use the formula above to compute the corresponding value of C_1. In 2D, the antisymmetric tensor of infinitesimal rotations reduces to a single L^2 scalar component p. Both p and all stress components have the same singularity at the origin corresponding to term $r^{-0.39596}$. The traction boundary data are reconstructed from the manufactured exact solution.

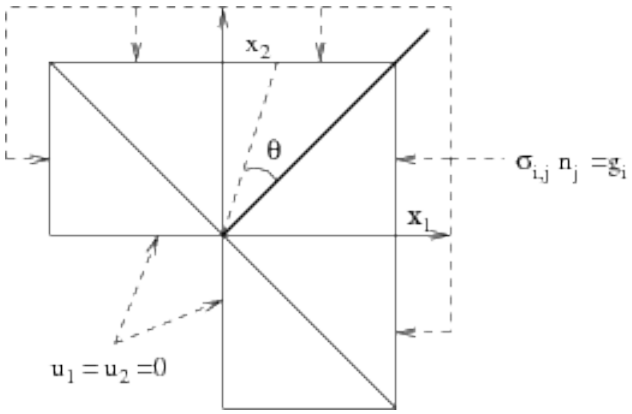

Figure 5: L-shape domain problem.

Since p and all stress components have the same singularity at the origin corresponding to term $r^{-0.39596}$, they all stay in Sobolev space $H^{1-0.39596-\epsilon}(\Omega) = H^{0.60404-\epsilon}(\Omega)$, for arbitrary small $\epsilon > 0$. According to L^2 best approximation results, the rate of convergence for uniform-h refinement is expected to be $h^{0.60404}$. For 2D uniform meshes, $h^2 \approx N^{-1}$, where N is the total number of degrees of freedom. This impies that the rate of convergence for uniform-h refinements in terms of the total number of d.o.f. should be $N^{-0.30202}$.

4.2.1 Mixed method results

In order to confirm the stability of the method, we have solved the problem using uniform, h-adaptive and hp-adaptive refinements. In all three cases, we start with a mesh consisting of six triangles of second order for the displacements and the infinitesimal rotation. The stresses are discretized with elements of one order higher. Both h- and hp-refinements are driven with the two mesh strategies discussed in detail in [12, 17]. Given a current (coarse) mesh, we refine it globally (in h for the h-refinements, and in both h and p for the hp-refinements) to obtain the corresponding fine mesh. The problem is then solved on the fine mesh, and the corresponding solution is used to determine an optimal refinement of the coarse mesh. For the h-adaptive method, this is just an implementational short cut. Similar results would have been obtained using any reasonable a-posteriori error estimate. For the hp-refinements, however, the strategy is based on maximizing the rate with which the PB interpolation error of the fine grid solution is decreasing. In our experience, the hp strategy based on a discrete minimization algorithm, delivers much better meshes than

strategies based on asymptotic arguments, including the simple flagging strategy used for the DPG method. Figures 6,7 and 8 present history of convergence for uniform, h-adaptive and hp-adaptive refinements. For each type of refinement, we report the actual and the *best approximation* error for the exact solution. The two curves are parallel which indicates h-stability and possibly hp-stability as well. Finally, Fig. 9 compares

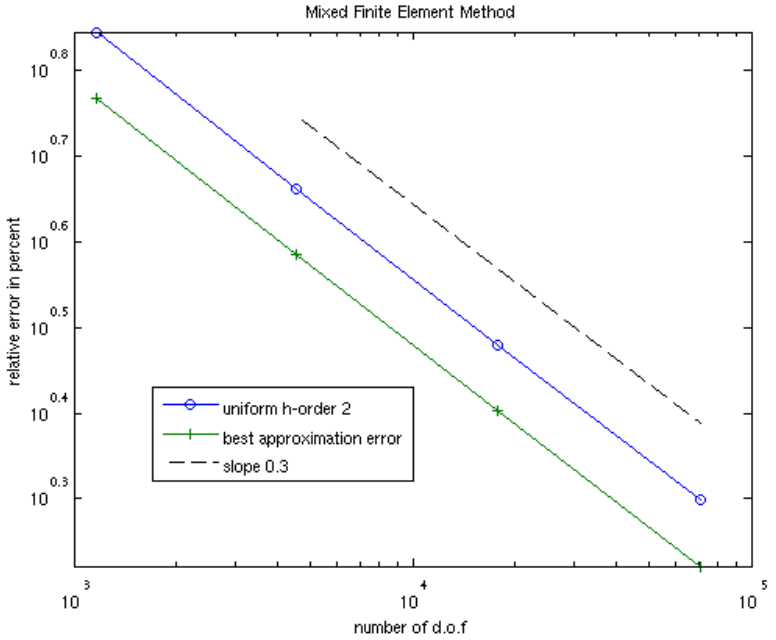

Figure 6: L-shape domain problem. Convergence history for the mixed method and uniform h-refinements. Comparison of the actual approximation and the best approximation errors.

the approximation errors for the three types of refinements. As expected, h-adaptivity restores the optimal rate of convergence. The hp-adaptivity produces the best results although, in the presented range, the rate seems to be still only algebraic.

4.2.2 DPG method results

Standard test norm. We begin with the version of the method based on the standard norm. Figures 10,11 and 12 present history of convergence for uniform, h-adaptive and hp-adaptive refinements using the energy and the L^2 norms. In all three cases, the two curves stay parallel to each other which indicates the stability of the method for general mesh refinements. The L^2-convergence error, however, is trailing almost two orders of magnitude behind the energy error. This is a bit surprising as the problem does not involve any small parameters (both material constants μ and λ are of order one). Figure 13 presents a comparison of all three refinements using the *relative* L^2-error. Recall that the required engineering accuracy is of order 1 percent error. The comparison reveals the standard facts: adaptive h-refinements restore the optimal rate of convergence, and adaptive hp-refinements produce better (possibly exponential ?) rates. Notice that p-

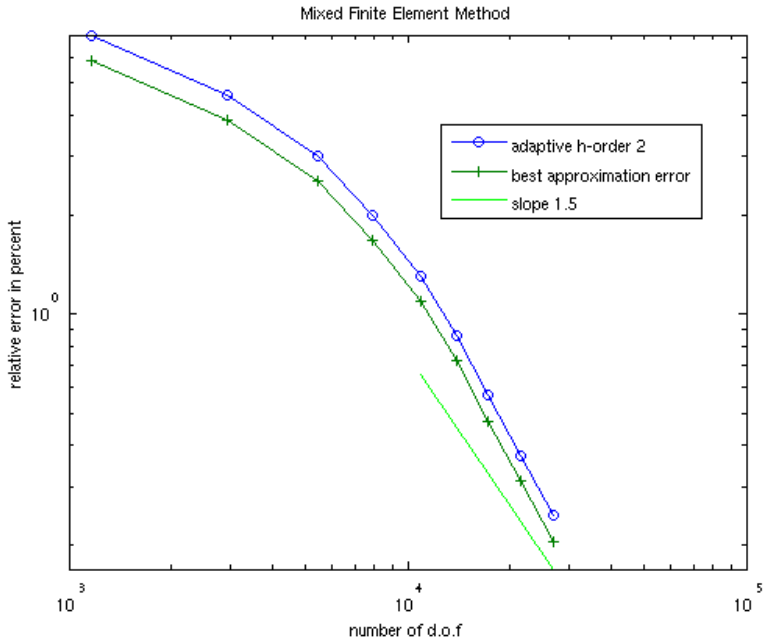

Figure 7: L-shape domain problem. Convergence history for the mixed method and h-adaptive refinements. Comparison of the actual approximation and the best approximation errors.

refinements have occurred only in the 8-th iteration; for the first 7 iterations, h- and hp-adaptivity produces the same results.

Optimal test norm. We repeat now the same experiments but with the optimal test norm discussed in Section 3. The first question to answer was the value of constant β controlling the zero order contribution to the optimal test norm 3.29. It was rather surprising to learn that for $\beta = 1$, the obtained results were practically of the same quality as for the standard norm. Smaller values of β produce better results but, with a decreasing value of β, we encountered round-off error effects, beginning to lose symmetry of element stiffness matrices. The results presented below were obtained with $\beta = 10^{-4}$. Despite the fact that the local problems were solved using Gaussian elimination with pivoting, we preserved the symmetry of element stiffness matrices in seven significant digits only.

Figures 14,15 and 16 present history of convergence for uniform, h-adaptive and hp-adaptive refinements using the energy and the L^2 norms. Again, the two curves stay parallel to each other which indicates the stability of the method for general mesh refinements. The L^2-convergence error this time, however, stays within 120 percent of the energy error. Figure 17 presents a comparison of all three refinements using again the *relative* L^2-error. The rates are the same as for the standard norm but, quantitatively, the results are much better. In particular, the hp method delivers 0.1% error with about of 70k d.o.f. For illustration, the optimal hp mesh obtained after the first 15 refinements, is presented in Fig 18.

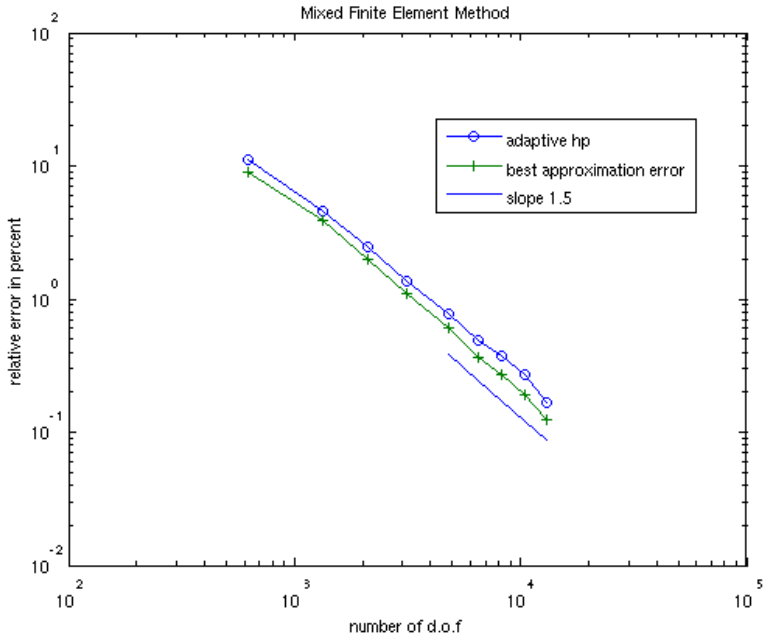

Figure 8: L-shape domain problem. Convergence history for the mixed method and hp-adaptive refinements. Comparison of the actual approximation and the best approximation errors.

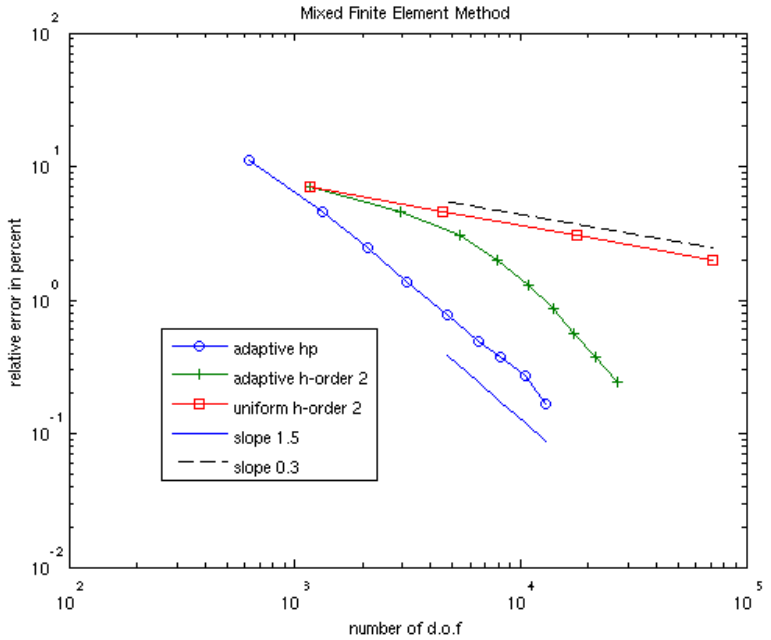

Figure 9: L-shape domain problem. Comparison of different refinement strategies for the mixed method.

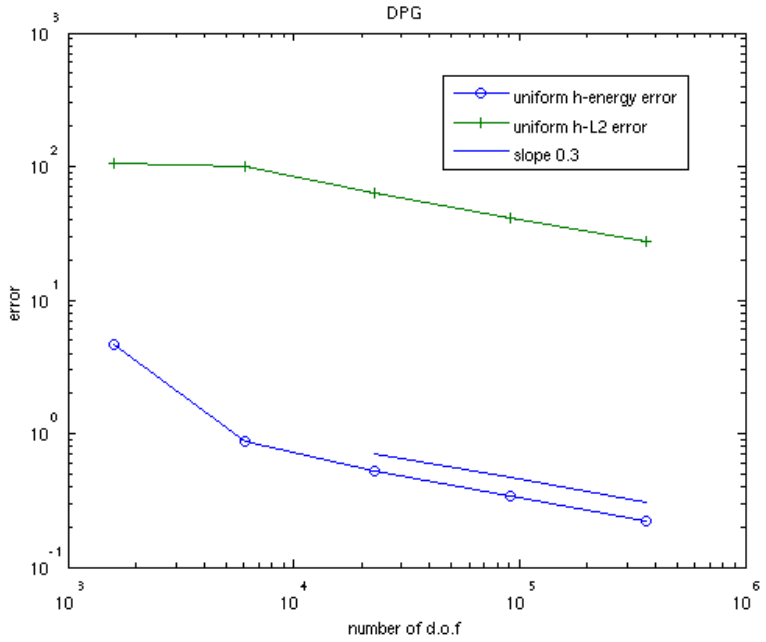

Figure 10: L-shape domain problem. Convergence history for standard test norm and uniform h-refinements.

4.3 Comparison of mixed and DPG methods

We conclude the presentation with a comparison of the mixed and DPG methods. Since the hp-adaptive strategies used in both cases were significantly different, we decided to use the adaptive h-refinements as a basis for comparison of the two methods. Notice that, for the L-shape domain problem, the stress is divergence free, and that this property is preserved for the discrete solution. Consequently, the $H(\mathrm{div})$-norm used in the stability analysis for the mixed method reduces in this case to the L^2-norm only. Fig. 19 presents the convergence history for the mixed method and the DPG method with the optimal test norm. The two curves go perfectly parallel to each other but the DPG method is trailing behind the mixed method by roughly a factor of 1.5, i.e. for the same number of d.o.f., the error corresponding to the mixed method is 1.5 smaller than that for the DPG method. This is related to the fact that DPG needs the additional d.o.f. for fluxes.

5 Conclusions

In the paper, we have presented a numerical comparison of two FE methods based on the dual-mixed formulation for linear elasticity: the mixed method of Arnold, Falk and Winther based on the formulation with weakly imposed symmetry, and the recent Discontinuous Petrov Galerkin (DPG) method proposed by

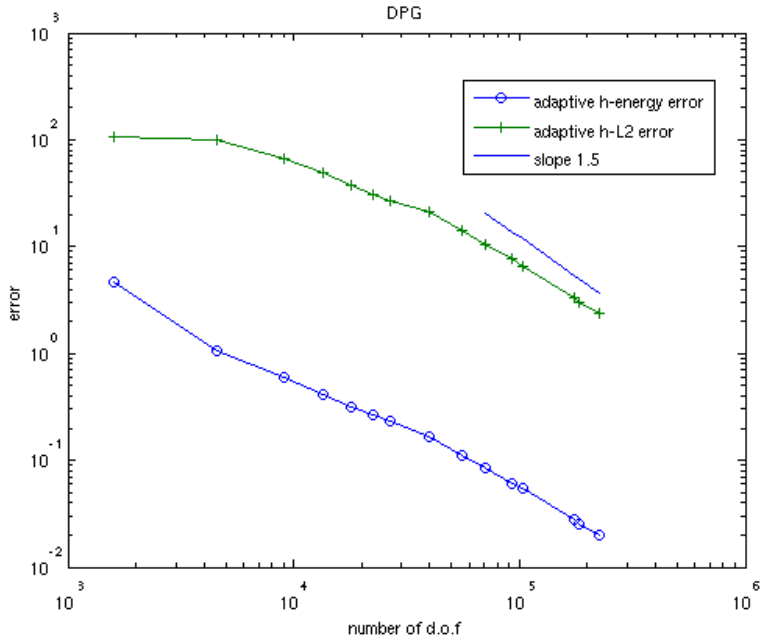

Figure 11: L-shape domain problem. Convergence history for standard test norm and h-adaptive refinements.

Demkowicz and Gopalakrishnan.

The numerical experiments indicate that both methods are stable for general hp meshes and, therefore, both discretizations seem to provide a basis for building hp-adaptive versions of the methods.

Proving stability of the p- and hp-versions of AFW element remains an open problem and, in context of our own work on the generalization to element of variable order, the issue does not look trivial.

The DPG method is based on three major assumptions.

(a) We assume that the underlying variational formulation is well-posed. This involves defining precisely energy spaces for the fluxes, and proving the inf-sup condition.

(b) In context of h-adaptivity, we assume that the method is uniformly stable with respect to mesh refinements. In other words, when we refine the mesh and introduce new interelement boundaries with new fluxes, the inf-sup constant should stay the same or, at least, uniformly bounded.

(c) The error in approximating the optimal test functions is either negligible or can be controlled via local, subelement adaptivity.

Except for the pure convection problem [14], the theoretical work for the multidimensional version of DPG is in its infancy. The presenting experiments shed some new light on the necessary numerical analysis. For

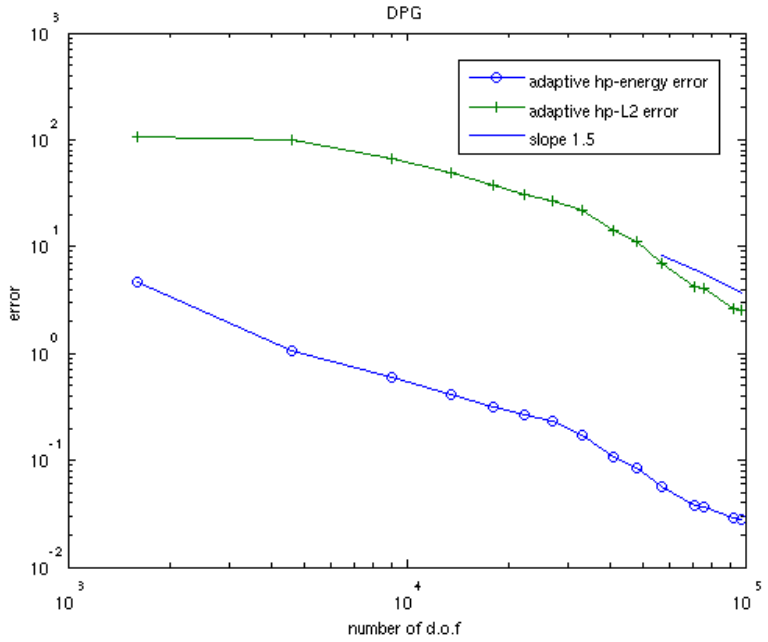

Figure 12: L-shape domain problem. Convergence history for standard test norm and hp-adaptive refinements.

instance, in context of h-refinements, the experiments indicate that it is necessary to use one order higher discretization for fluxes than for the field variables.

The DPG method offers two great perspectives: stability of p-refinements, and the possibility of producing almost best L^2 approximation, with the optimal test norm. Replacing the interface terms in the formula for the optimal norm needs to be analyzed. Two things surprised us: the fact that the standard test norm leads to a small inf-sup constant, and that the coefficient β in the optimal norm has to be so small to make the energy norm close to the L^2-norm.

We hope to produce new numerical evidence and analysis soon.

In summary, the numerical evidence indicates that both methods exhibit optimal stability in context of general hp-refinements with stability constants of order one.

References

[1] M. Amara and J. M. Thomas. Equilibrium finite elements for the linear elastic problem. *Numer. Math.*, 33:367–383, 1979.

[2] D. N. Arnold, F. Brezzi, and J. Douglas. Peers: a new mixed finite element for plane elasticity. *Japan J. Appl. Math.*, 1:347–367, 1984.

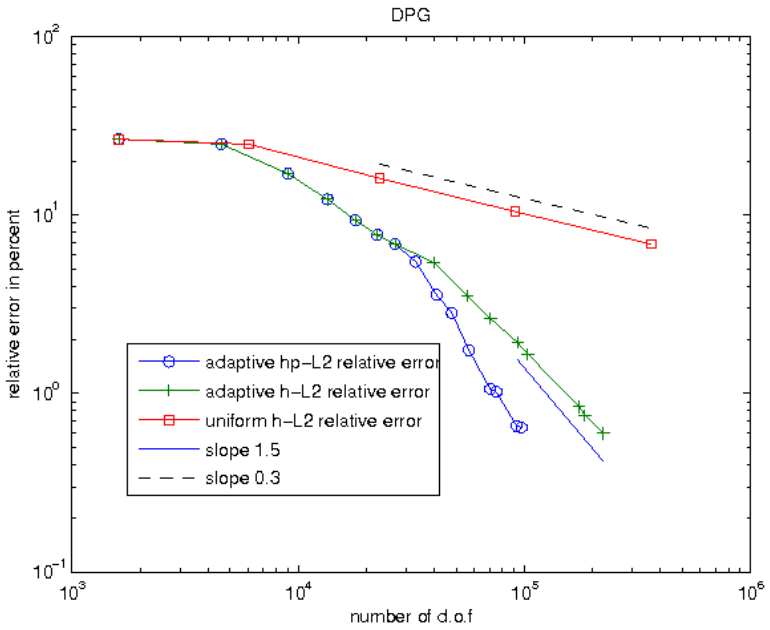

Figure 13: L-shape domain problem. Comparison of different refinement strategies for the DPG method with standard norm. Relative L^2-error vs. number of d.o.f.

[3] D. N. Arnold and R. S. Falk. A new mixed formulation for elasticity. *Numer. Math.*, 53:13–30, 1988.

[4] D. N. Arnold, R. S. Falk, and R. Winther. Finite element exterior calculus, homological techniques, and applications. *Acta Numer.*, pages 1–155, 2006.

[5] D. N. Arnold, R. S. Falk, and R. Winther. Mixed finite element methods for linear elasticity with weakly imposed symmetry. *Mathematics of Computation*, 76:1699–1723, 2007.

[6] C.L. Bottasso, S. Micheletti, and R. Sacco. The discontinuous Petrov-Galerkin method for elliptic problems. *Comput. Methods Appl. Mech. Engrg.*, 191:3391–3409, 2002.

[7] C.L. Bottasso, S. Micheletti, and R. Sacco. A multiscale formulation of the discontinuous Petrov-Galerkin method for advective-diffusive problems. *Comput. Methods Appl. Mech. Engrg.*, 194:2819–2838, 2005.

[8] P. Causin and R. Sacco. A discontinuous Petrov-Galerkin method with Lagrangian multipliers for second order elliptic problems. *SIAM J. Numer. Anal.*, 43, 2005.

[9] P. Causin, R. Sacco, and C.L. Bottasso. Flux-upwind stabilization of the discontinuous Petrov-Galerkin formulation with Lagrange multipliers for advection-diffusion problems. *M2AN Math. Model. Numer. Anal.*, 39:1087–1114, 2005.

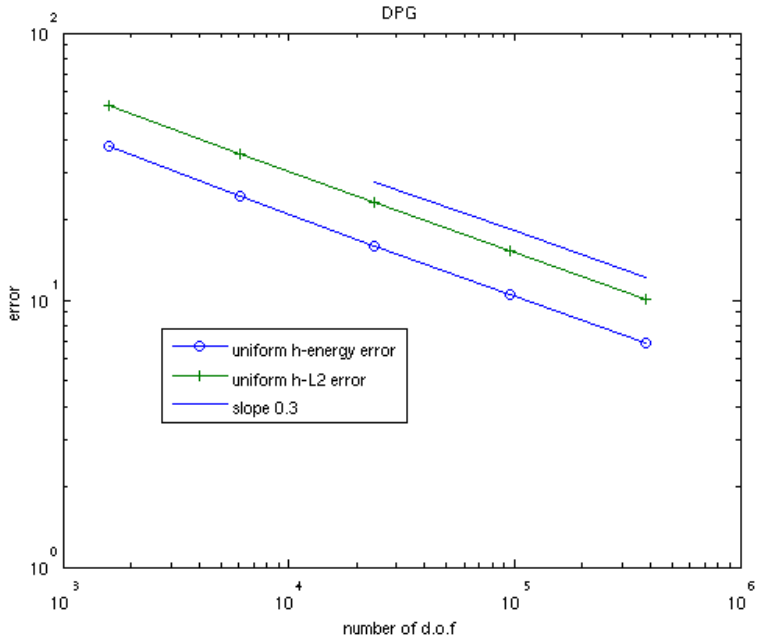

Figure 14: L-shape domain problem. Convergence history for optimal test norm and uniform h-refinements.

[10] B. Cockburn, J. Gopalakrishnan, and J. Guzman. A new elasticity element made for enforcing weak stress symmetry. *Mathematics of Computation*, 2009.

[11] B. M. Fraeijs de Veubeke. Stress function approach. *Proc. of the World Congress on Finite Element Methods in Structural Mechanics*, 5:J.1–J.51, 1975.

[12] L. Demkowicz. *Computing with hp Finite Elements. I.One- and Two-Dimensional Elliptic and Maxwell Problems*. Chapman & Hall/CRC Press, Taylor and Francis, October 2006.

[13] L. Demkowicz. Polynomial exact sequences and projection-based interpolation with applications to Maxwell equations. In D. Boffi and L. Gastaldi, editors, *Mixed Finite Elements, Compatibility Conditions and Applications*, volume 1939 of *Lecture Notes in Mathematics*, pages 101–158. Springer-Verlag, 2008. see also ICES Report 06-12.

[14] L. Demkowicz and J. Gopalakrishnan. A class of discontinuous Petrov-Galerkin methods. Part I: The transport equation. *Comput. Methods Appl. Mech. Engrg.*, 2009. accepted, see also ICES Report 2009-12.

[15] L. Demkowicz and J. Gopalakrishnan. A class of discontinuous Petrov-Galerkin methods. Part II: Optimal test functions. Technical Report 16, ICES, 2009. Numer. Meth. Part. D. E., in review.

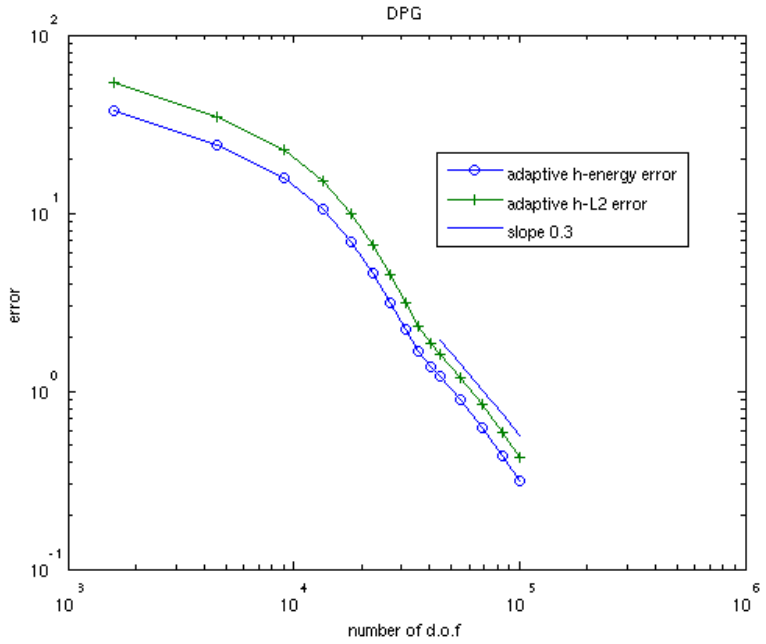

Figure 15: L-shape domain problem. Convergence history for optimal test norm and uniform h-refinements.

[16] L. Demkowicz, J. Gopalakrishnan, and A. Niemi. A class of discontinuous Petrov-Galerkin methods. Part III: Adaptivity. Technical Report 1, ICES, 2010.

[17] L. Demkowicz, J. Kurtz, D. Pardo, M. Paszyński, W. Rachowicz, and A. Zdunek. *Computing with hp Finite Elements. II. Frontiers: Three-Dimensional Elliptic and Maxwell Problems with Applications*. Chapman & Hall/CRC, October 2007.

[18] R. S. Falk. Finite element methods for linear elasticity. In *Lecture Notes in Mathematics*, pages 160–194. Springer-Verlag, 2008.

[19] M. Farhloul and M. Fortin. Dual hybrid methods for the elasticity and the Stokes problem: a unified approach. *Numer. Math.*, 76:419–440, 1997.

[20] M. E. Morley. A family of mixed finite elements for linear elasticity. *Numer. Math.*, 55:633–666, 1989.

[21] A.H. Niemi, J.A. Bramwell, and L.F. Demkowicz. Discontinuous Petrov-Galerkin method with optimal test functions for thin-body problems in solid mechanics. Technical Report 13, ICES, 2010.

[22] W. Qiu and L. Demkowicz. Mixed $\boldsymbol{hp}$-finite element method for linear elasticity with weakly imposed symmetry. *Comput. Methods Appl. Mech. Engrg.*, 198:3682–3701, 2009.

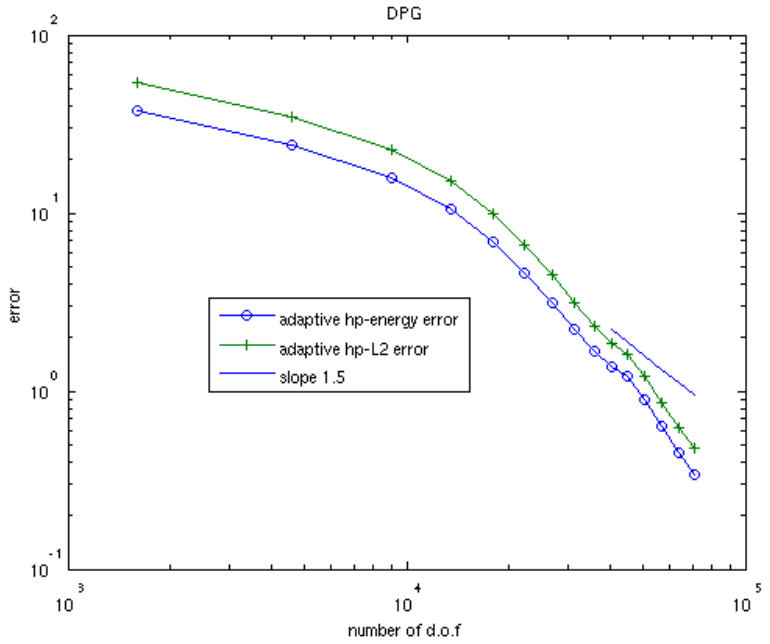

Figure 16: L-shape domain problem. Convergence history for optimal test norm and adaptive h-refinements.

[23] W. Qiu and L. Demkowicz. Mixed hp-finite element method for linear elasticity with weakly imposed symmetry II: Curvilinear elements in 2D. Technical Report 6, ICES, 2010.

[24] W. Qiu and L. Demkowicz. Mixed hp-finite element method for linear elasticity with weakly imposed symmetry III: stability analysis in 3d. Technical report, ICES, 2010. in preparation.

[25] E. Stein and R. Rolfes. Mechanical conditions for stability and optimal convergence of mixed finite elements for linear plane elasticity. *Comput. Methods Appl. Mech. Engrg.*, 84:77–95, 1990.

[26] R. Stenberg. On the construction of optimal mixed finite element methods for the linear elasticity problem. *Numer. Math.*, 48:447–462, 1986.

[27] R. Stenberg. A family of mixed finite elements for the elasticity problem. *Numer. Math.*, 53:513–538, 1988.

[28] R. Stenberg. Two low-order mixed methods for the elasticity problem. *The Mathematics of Finite Elements and Applications, VI*, pages 271–280, 1988.

[29] D. Vasilopoulos. On the Determination of Higher Order Terms of Singular Elastic Stress Fields near Corners. *Numer. Math.*, 53:51–95, 1988.

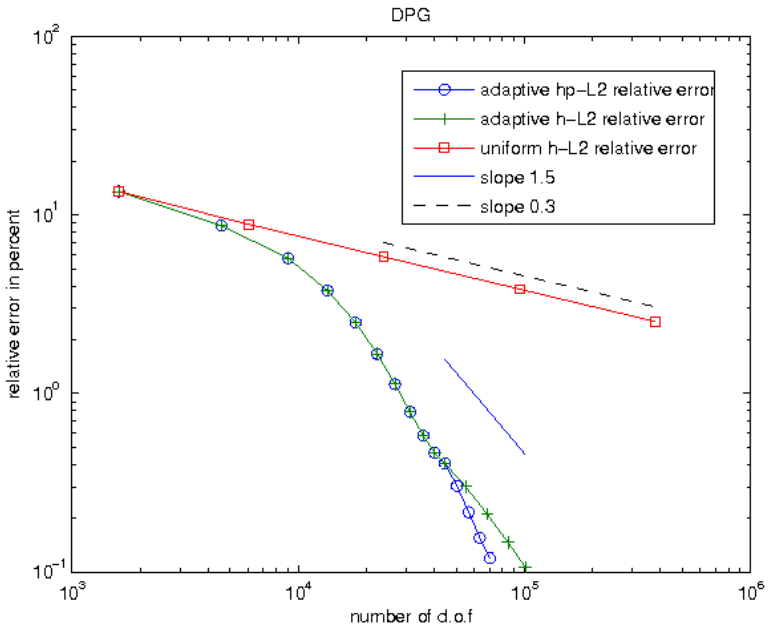

Figure 17: L-shape domain problem. Convergence history for optimal test norm and adaptive hp-refinements.

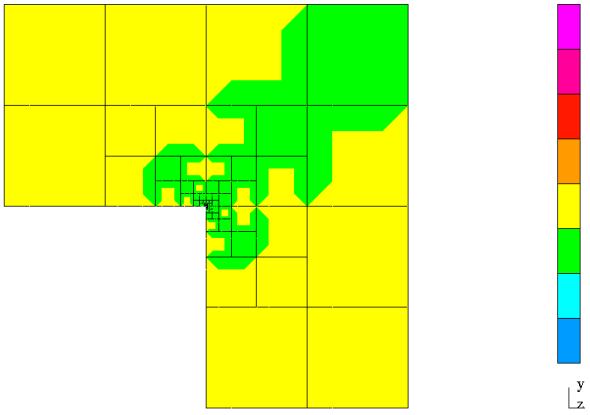

Figure 18: L-shape domain problem. Optimal hp mesh obtained after 15 refinements, corresponding to 0.1% relative L^2 error.

[30] J. Zitelli, I. Muga, L. Demkowicz, J. Gopalakrishnan, D. Pardo, and V. Calo. A class of discontinuous Petrov-Galerkin methods. Part IV: Wave propagation problems. Technical Report 17, ICES, 2010.

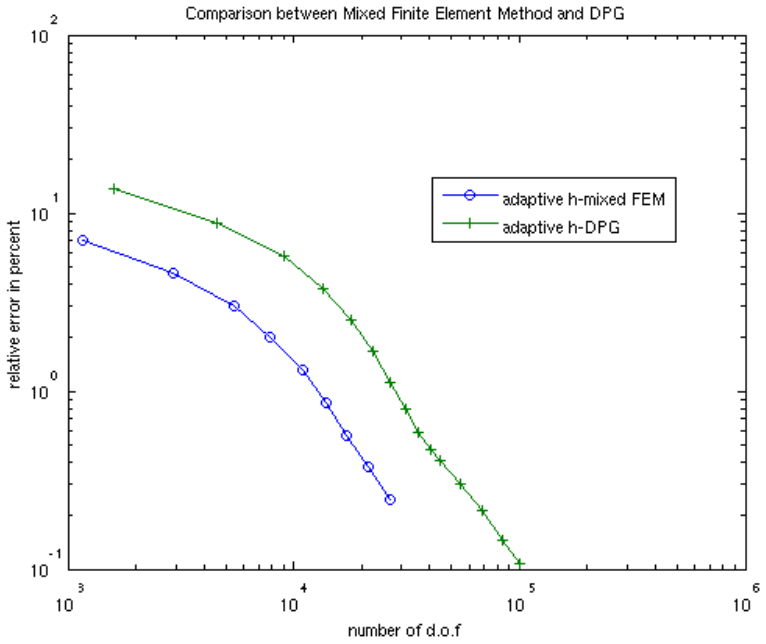

Figure 19: L-shape domain problem. Adaptive h-refinements. Comparison of mixed and DPG methods using relative L^2-norm.